Syntheses, Crystal Structures and Magnetic Properties of Two Nickel(II) Compounds with 4,4′-Bipyridine Ligands

Xiao-Ke Yu, Xiang-Sheng Zhai, Yue-Qing Zheng, and Hong-Lin Zhu

Center of Applied Solid State Chemistry Research, Ningbo University, Ningbo, 315211, P. R. China

Reprint requests to Prof. Dr. Yue-Qing Zheng. Fax: Int. +574/87600747.
E-mail: yqzhengmc@163.com

Z. Naturforsch. **2014**, *69b*, 62 – 70 / DOI: 10.5560/ZNB.2014-3242
Received September 22, 2013

Hydrothermal reactions of 4,4′-bipyridine, benzoic acid/*p*-methylbenzoic acid, $Ni(NO_3)_2 \cdot 6H_2O$ and NH_4OH yielded $[Ni(bpy)_{1.5}(H_2O)_2(BA)_2]\cdot H_2O$ (**1**) and $[Ni(bpy)(HMBA)(MBA)_2]_n$ (**2**) (bpy = 4,4′-bipyridine, HBA = benzoic acid, HMBA = *p*-methylbenzoic acid). The Ni(II) ions of compound **1** are six-coordinated and bridged by 4,4′-bipyridine ligands to form a binuclear structure while complex **2** features polymeric chains which are connected by 4,4′-bipyridine molecules. Variable-temperature magnetic susceptibility measurements from 300 to 30 K showed the presence of weak ferromagnetic interactions between the Ni(II) ($S = 1$) ions *via* the 4,4′-bipyridine bridges.

Key words: Ni(II) Complexes, Hydrothermal Reactions, Benzoic Acid, Bipyridyl, Magnetism

Introduction

Supramolecular systems have attracted considerable attention, not only for their various structure features, but also for their potential applications in gas storage and separation, magnetic devices, molecular recognition *etc.* [1 – 11]. Supramolecular assemblies can be designed and constructed based on non-covalent intermolecular interactions such as, among others, hydrogen bonds, aromatic π-π-stacking, electrostatic and van der Waals forces. The judicious choice of special inorganic and organic building blocks is the key steps for manipulating the network structure of such materials. Aromatic carboxylic acids, such as benzoic *m*-nitrobenzoic acid, *o*-phthalic, *m*-phthalic and *p*-phthalic acids, have been shown to produce a great variety of interesting structures [12 – 30], because they can not only coordinate metal ions in a variety of ways but also act as a hydrogen-bond acceptors, taking part in the formation of polymeric networks [31].

Our efforts to explore supramolecular nickel(II) complexes with aromatic carboxylic acid and 4,4′-bipyridine resulted in the preparation of two new nickel coordination polymers: $[Ni(bpy)_{1.5}(H_2O)_2(BA)_2]\cdot H_2O$ (**1**) and $[Ni(bpy)(HMBA)(MBA)_2]_n$ (**2**) (bpy = 4,4′-bipyridine, HBA = benzoic acid, HMBA = *p*-methylbenzoic acid). Their single-crystal X-ray structures, magnetic properties, infrared spectra and thermal degradation are discussed herein.

Results and Discussion

Description of the crystal structures

*$[Ni(bpy)_{1.5}(H_2O)_2(BA)_2]\cdot H_2O$ (**1**)*

Complex **1** crystallizes in the triclinic space group $P\bar{1}$, and the asymmetric unit contains one Ni(II) ion, one and a half 4,4′-bipyridine molecules (bpy), two benzoate anions (BA^-), two aqua ligands and one guest water molecule (Tables 1, 2). As shown in Fig. 1, the Ni(II) ion is six-coordinated defined by two oxygen atoms from two BA^-, two hydroxyl oxygen atoms from aqua ligands and two nitrogen atoms from different bpy ligands forming an octahedral unit NiN_2O_4 with the distances in the range of Ni–O = 2.046 – 2.099 Å, Ni–N = 2.114 and 2.119 Å (Table 2). The *cisoid* and *transoid* bond angles fall in the region 84.7 – 93.9° and 174.9 – 177.4°, respectively, and they deviate from the ideal values, indicating the octahedral coordination to be slightly distorted. The average Ni–N and Ni–O bond lengths are 2.117 Å and

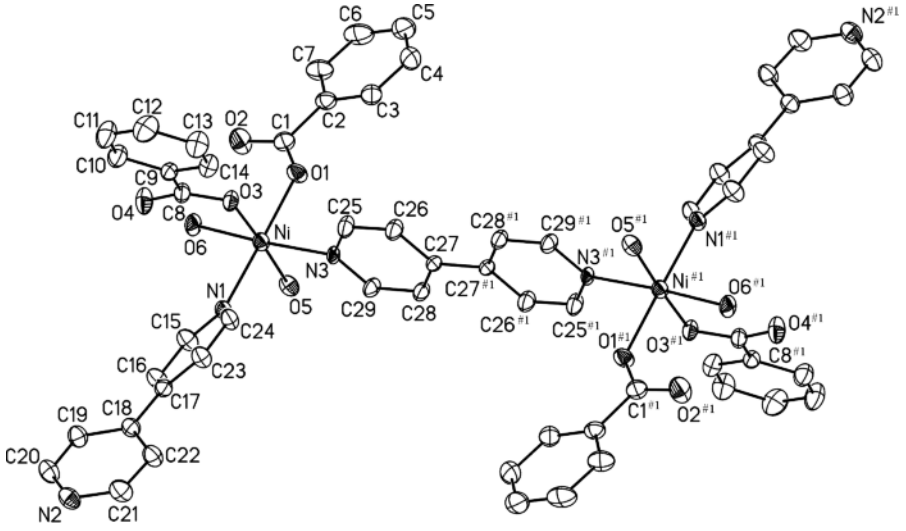

Fig. 1. ORTEP view of the coordination environment of the Ni(II) ion in $[Ni(bpy)_{1.5}(H_2O)_2(BA)_2]\cdot H_2O$ (**1**) with 45% displacement ellipsoids (symmetry code: #1 = $2-x$, $1-y$, $1-z$).

Table 1. Crystal structure data for **1** and **2**.

	1	**2**
Empirical formula	$C_{29}H_{28}N_3NiO_7$	$C_{34}H_{29}N_2NiO_6$
M_r	589.26	621.31
Crystal size, mm^3	$0.32\times0.22\times0.13$	$0.48\times0.44\times0.23$
Crystal system	triclinic	monoclinic
Space group	$P\bar{1}$	$P2_1/n$
a, Å	8.033(2)	10.653(2)
b, Å	12.477(3)	24.370(5)
c, Å	14.756(3)	11.276(2)
α, deg	71.74(3)	90.0
β, deg	76.44(3)	94.72(3)
γ, deg	86.88(3)	90.0
V, Å^3	1365.1(5)	2917.6(10)
Z	2	4
$D_{calcd.}$, g cm^{-3}	1.43	1.41
$\mu(MoK_\alpha)$, cm^{-1}	0.8	0.7
$F(000)$, e	614	1296
hkl range	$\pm10, \pm16, \pm19$	$\pm13, \pm31, \pm14$
$((\sin\theta)/\lambda)_{max}$, Å^{-1}	0.65	0.65
Refl. measured/unique/	13201/6143/	27618/6565/
R_{int}	0.043	0.06
Param. refined	364	388
$R(F)/wR(F^2)$[a,b] (all refls)	0.0932/0.1338	0.0677/0.1201
GoF (F^2)[c]	1.175	1.091
$\Delta\rho_{fin}$ (max/min), e Å^{-3}	0.92/−0.86	0.09/−0.86

[a] $R(F) = \Sigma||F_o| - |F_c||/\Sigma|F_o|$; $wR(F^2) = [\Sigma w(F_o^2 - F_c^2)^2/\Sigma w(F_o^2)^2]^{1/2}$; GoF $= [\Sigma w(F_o^2 - F_c^2)^2/(n_{obs} - n_{param})]^{1/2}$; $w = [\sigma^2(F_o^2) + (aP)^2 + bP]^{-1}$, where $P = (\mathrm{Max}(F_o^2, 0) + 2F_c^2)/3$; for **1**: $a = -0.0175$, $b = 2.1407$; for **2**: $a = 0.0484$, $b = 1.7884$.

Table 2. Selected bond lengths (Å), and angles (deg) for **1** with estimated standard deviations in parentheses[a].

Distances			
Ni–O1	2.046(3)	Ni–O6	2.099(3)
Ni–O3	2.070(3)	Ni–N1	2.119(3)
Ni–O5	2.078(3)	Ni–N3	2.114(3)
Angles			
O1–Ni–O3	89.7(1)	O3–Ni–N3	90.5(1)
O1–Ni–O5	92.9(1)	O5–Ni–O6	87.4(1)
O1–Ni–O6	90.8(1)	O5–Ni–N1	91.2(1)
O1–Ni–N1	175.7(1)	O5–Ni–N3	90.4(1)
O1–Ni–N3	84.7(1)	O6–Ni–N1	90.8(1)
O3–Ni–O5	177.4(1)	O6–Ni–N3	174.9(1)
O3–Ni–O6	91.9(1)	N1–Ni–N3	93.9(1)
O3–Ni–N1	86.3(1)		

Hydrogen bonding contacts

D–H	d(D–H)	d(H···A)	d(D–H···A)	∠(D–H···A)	A
O5–H5B	0.86	1.88	2.744(5)	177	N2$^{\#2}$
O5–H5C	0.82	2.08	2.761(5)	141	O7$^{\#3}$
O6–H6B	0.86	1.79	2.627(4)	165	O4
O6–H6C	0.88	1.86	2.617(5)	144	O2
O7–H7B	0.84	2.08	2.889(5)	161	O6$^{\#3}$
O7–H7C	0.86	1.92	2.731(5)	156	O4

[a] Symmetry transformations used to generate equivalent atoms: #2 $x, 1+y, z$; #3 $1-x, 1-y, -z$.

2.073 Å, respectively, which are close to literature values [32–34].

The Ni(II) atoms are bridged by 4,4′-bipyridine groups to form binuclear units, arranged around an inversion center. In the [001] direction, the dimers are linked *via* hydrogen bonds with the guest water molecule (O7–H7C···O4 and O7–H7B···O6$^{\#2}$, #2 = $1-x, 1-y, -z$) into supramolecular chains (Fig. 2), which are further linked by π-π stacking (the face-to-face distances between the BA$^-$ and unbridged bpy

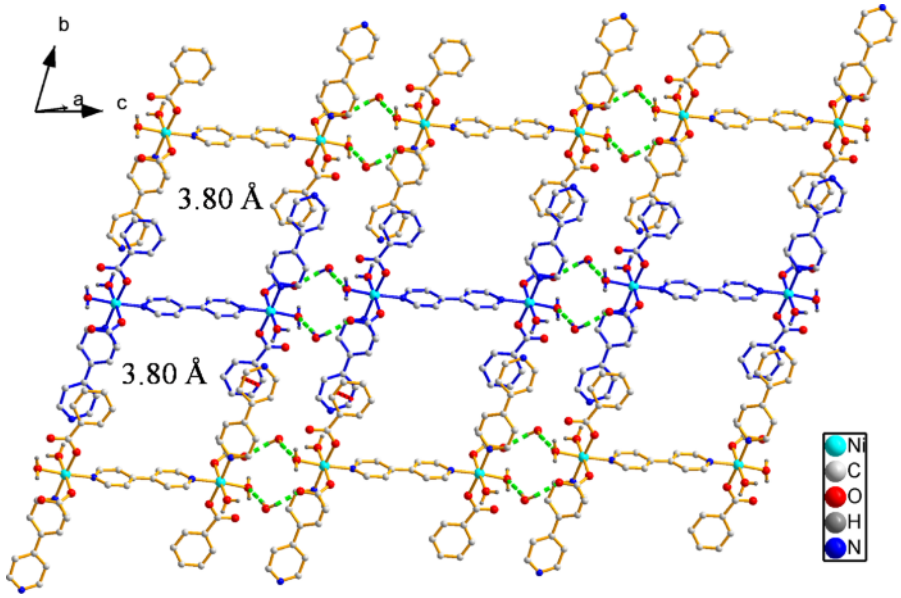

Fig. 2 (color online). Layers connected by O–H···O hydrogen bonding and π-π stacking in crystals of **1**.

aromatic rings being 3.8 Å) into layers parallel to the $(\bar{1}11)$ plane (Fig. 2). The layers are arranged alternately in an ···ABAB··· sequence and further assembled into a three-dimensional network by aromatic stacking interactions, the face-to-face distances between BA^- and bridging bpy benzene rings being 3.7 Å.

*[Ni(bpy)(HMBA)(MBA)$_2$]$_n$ (**2**)*

Compound **2** crystallizes in the space group $P2_1/n$, and the asymmetric unit consists of a Ni(II) ion, one 4,4′-bipyridine molecule (bpy), two *p*-methylbenzoate anions (namely MBA1 and MBA2 containing the oxygen atoms O1/O2 and O5/O6, respectively) and one molecule of coordinated *p*-methylbenzoic acid HMBA containing the oxygen atoms O3/O4 (Tables 1 and 3). Two carboxyl oxygen atoms O1 and O3 of MBA1 and HMBA are monodentate to the Ni(II) atom, while MBA2 is a bidentate chelating ligand. As shown in Fig. 3, Ni(II) is in an octahedral geometry, coordinated by two nitrogen atoms from bpy ligands, two oxygen atoms from MBA2 and one oxygen atom from MBA1 and HMBA each. The Ni atoms display Ni–O/N bond lengths in the range of Ni–O/N = 2.02(1) – 2.13(1) Å. The *cisoid* and *transoid* bond angles fall in the regions 61.8(1) – 110.2(1)° and 155.1(1) – 177.4(1)°, respectively, indicating the octahedral coordination to be distorted.

The [Ni(bpy)(HMBA)(MBA)$_2$]$_n$ molecules are bpy-bridged to give rise to a chain structure along the [001] direction (Fig. 4). The one-dimensional Ni(II) coordination polymers $^1_\infty$[Ni(bpy)(HMBA)(MBA)$_2$] are connected through offset face-to-face π-π stacking interactions with a mean interplanar distance of 3.35 Å between MBA1 and HMBA to generate a two-dimensional network parallel to (010) (Fig. 4). The MBA2 groups are almost perpendicular to the layer on both sides. Along the [010] direction, each MBA2 of one layer protrudes into the void between two adjacent *p*-methylbenzoic acid groups of the neighboring layers, so that the layers are stacked to form bi-layers. The bi-layers are stabilized by intermolecular π-π stacking interactions between *p*-methylbenzoic acid ligands (mean inter-planar distances are 3.45 and 3.50 Å). The bi-layers are arranged alternately in an ···ABAB··· sequence and further assembled into a three-dimensional network by van der Waals forces.

A comparison of the dinuclear complex [Ni(bpy)$_{1.5}$(H$_2$O)$_2$(BA)$_2$]·H$_2$O (**1**) with the previously obtained 1D complex [Ni(bpy)(H$_2$O)$_2$(BA)$_2$]$_n$ [18] is particularly worthwhile. The compounds differ only in the bpy content apart from a co-crystallized water molecule with key structural features being similar. In the complex [Ni(bpy)(H$_2$O)$_2$(BA)$_2$]$_n$, there are two molecules of bpy per dimer while in **1** there are three bpy per dimer. Slow evaporation of

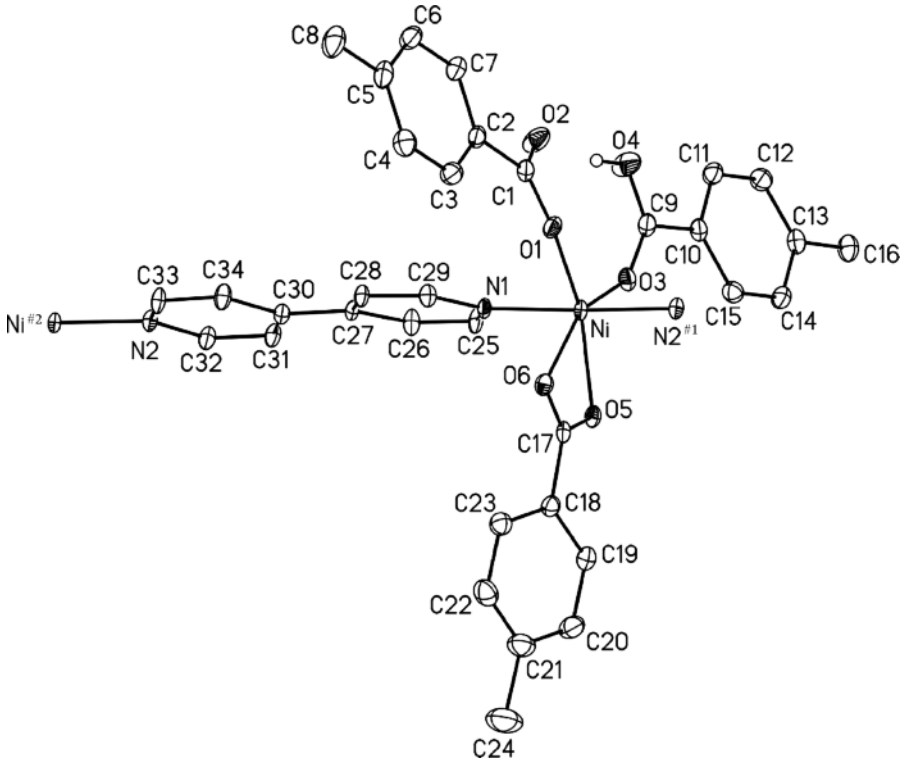

Fig. 3. ORTEP view of the complex $[Ni(bpy)(HMBA)(MBA)_2]_n$ (**2**) with displacement ellipsoids (45 % probability) and atomic labeling (symmetry codes: #1 = x, y, $1+z$; #2 = x, y, $1-z$).

mixed solvent (acetone, MeOH and EtOH) from the reaction mixture yielded 1D $[Ni(bpy)(H_2O)_2(BA)_2]_n$ in a diffusion-controlled reaction while **1** was obtained by hydrothermal synthesis in aqueous solution. Table 4 gives a concise summary of the reaction conditions leading to $[Ni(bpy)(H_2O)_2(BA)_2]_n$ [18], **1** and **2**. Thus the main reasons leading to the different compositions of these complexes may be temperature and pressure.

The new complexes **1** and **2** were both prepared by hydrothermal methods with HMBA being used for **2** instead of HBA. Obviously, their structural differences are mainly due to the different substitution pattern of the bencoic acid.

Table 3. Selected bond lengths (Å), and angles (deg) for **2** with estimated standard deviations in parentheses[a].

Distances			
Ni–O1	2.021(2)	Ni–O6	2.132(2)
Ni–O3	2.029(2)	Ni–N1	2.088(2)
Ni–O5	2.125(2)	Ni–N2$^{\#1}$	2.076(2)
Angles			
O1–Ni–O3	110.1(1)	O3–Ni–N2$^{\#1}$	89.2(1)
O1–Ni–O5	157.4(1)	O5–Ni–O6	62.2(1)
O1–Ni–O6	95.2(1)	O5–Ni–N1	90.8(1)
O1–Ni–N1	89.0(1)	O5–Ni–N2$^{\#1}$	91.4(1)
O1–Ni–N2$^{\#1}$	88.9(1)	O6–Ni–N1	90.3(1)
O3–Ni–O5	92.5(1)	O6–Ni–N2$^{\#1}$	90.6(1)
O3–Ni–O6	154.7(1)	N1–Ni–N2$^{\#1}$	177.8(1)
O3–Ni–N1	90.9(1)		

[a] Symmetry transformations used to generate equivalent atoms: #1 x, y, $1+z$.

PXRD

The products **1** and **2** were checked by PXRD, and the experimental and simulated PXRD patterns are shown in Fig. S1 (Supporting Information, available online; see note at the end of the paper for availability). Their peak positions are in good agreement with each other, indicating good phase purity of the bulk samples. The difference in intensity may be due to the preferred orientations in the powder samples.

Table 4. Summary of synthesis conditions leading to complexes $[Ni(bpy)(H_2O)_2(BA)_2]_n$ [18], **1** and **2**.

Synthesis	Synthesis condition	Complexes	Ref.
Diffusion	upper layer 4,4′-bpy acetone + MeOH + EtOH lower layer $Ni(NO_3)_2 \cdot 6H_2O$, $BANH_4$ H_2O	$[Ni(bpy)(H_2O)_2(BA)_2]_n$ 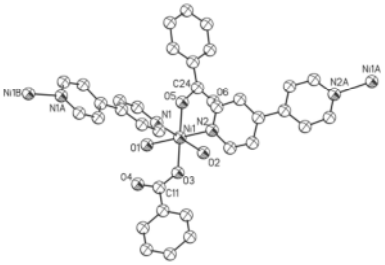	[18]
Hydrothermal	HBA, $Ni(NO_3)_2 \cdot 6H_2O$, 4,4′-bpy, $NH_3 \cdot H_2O$, H_2O 453 K, 3 d	$[Ni(bpy)_{1.5}(H_2O)_2(BA)_2] \cdot H_2O$ (**1**) 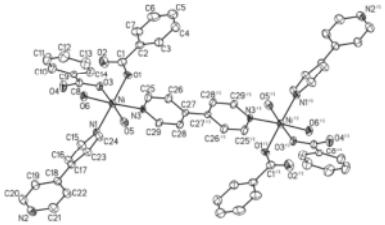	this work
Hydrothermal	HMBA, $Ni(NO_3)_2 \cdot 6H_2O$, 4,4′-bpy, $NH_3 \cdot H_2O$, H_2O 453 K, 3 d	$[Ni(bpy)(HMBA)(MBA)_2]_n$ (**2**) 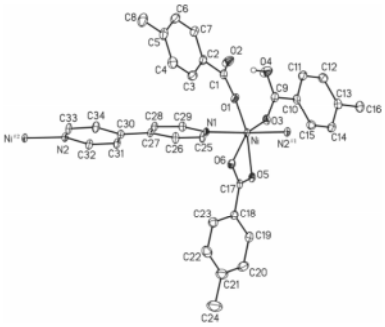	this work

Infrared spectra

As shown in Fig. S2 (Supporting Information), the IR spectra of the title complexes are in agreement with the key structural characteristics as shown above. For **1**, the IR spectrum shows broad bands centered at 3502 and 3294 cm^{-1}, indicating the presence of water in the complex. The strong absorption bands centered at 1598 and 1556 cm^{-1} for **1**, 1630, 1607 and 1571 cm^{-1} for **2**, can be ascribed to the asymmetric stretching vibration of the -COO groups, while the symmetric stretching vibration of the -COO groups results in absorptions at 1413 and 1392 cm^{-1} for **1**, 1541, 1512 and 1427 cm^{-1} for **2**. The separations are 185 and 164 cm^{-1} respectively for **1**, 89 – 144 cm^{-1} for **2**, of which the values of **1** correspond to monodentate coordination modes of the carboxylate groups and the value of **2** corresponds to mono- and bidentate modes of the carboxylate groups [35], which agrees well with the X-ray structural analyses. Both for **1** and **2**, the absorptions in the range 600 – 900 cm^{-1} can be attributed to the out-of-plane C–H vibrations of the organic ligand.

Thermal analysis

The TG curves are depicted in Fig. S3 (Supporting Information). Thermogravimetric analysis of complex **1** shows that the weight loss of the first step between 59 – 115 °C is 8.6 % in good agreement with the value of 9.2 % calculated for three moles H_2O per

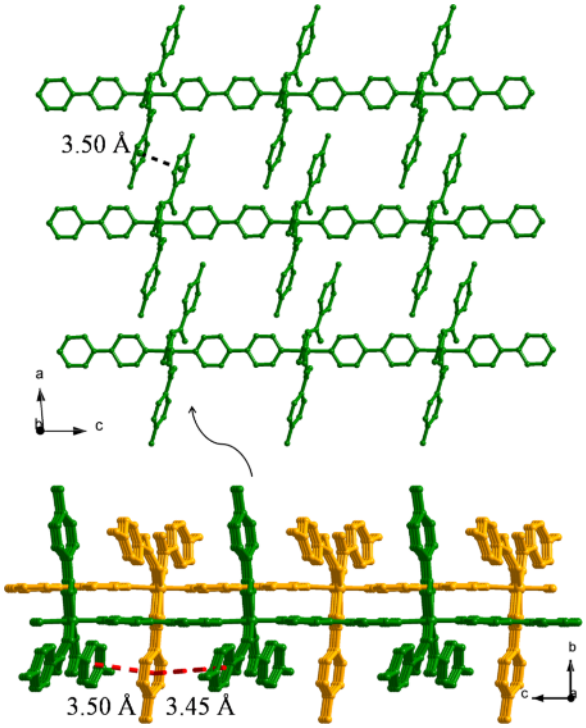

Fig. 4 (color online). 2D supramolecular network in crystals of **2**.

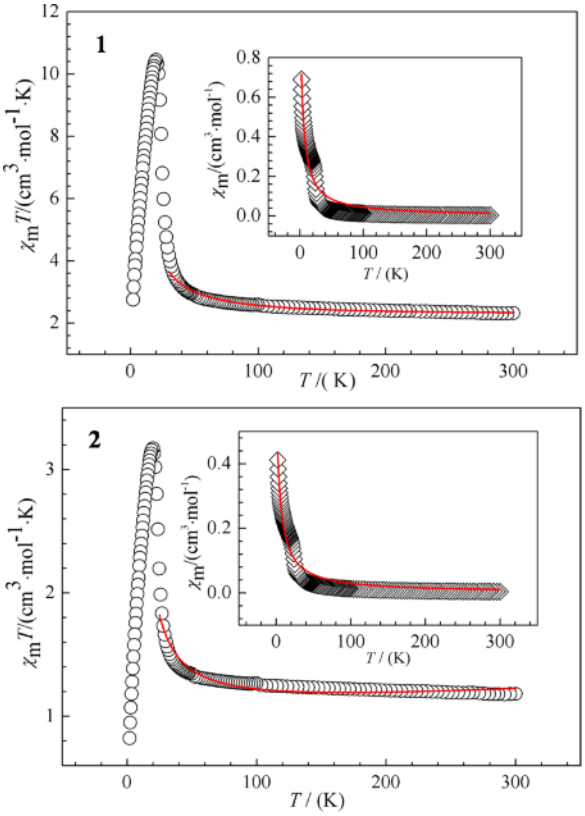

Fig. 5 (color online). Temperature dependence of the magnetic susceptibilities of **1** and **2**.

formula, implying complete dehydration. The second weight loss between 120 – 188 °C reaches 13.0 % close to the calculated value 13.3 % for removal of half of the 4,4′-bipyridine ligands. Upon heating, the observed weight loss of 61.7 % over 188 – 420 °C corresponds to decomposition of benzoic acid and release of all 4,4′-bipyridine. When further heated, the resulting intermediate loses weight very slowly. Thermal analysis shows **2** to be stable below 191 °C, at which temperature decomposition starts. The weight loss reaches 78.3 % at 409 °C. When further heated, the residue loses weight very slowly.

Magnetic properties

Temperature-dependent magnetic susceptibility measurements on compounds **1** and **2** were performed on polycrystalline samples in the temperature range of 2 – 300 K in a fixed magnetic field of 1 KOe (1 kOe = 7.96×10^4 A m^{-1}). The magnetic behavior presented in the form of $\chi_M T$ and χ_M *versus* T plots is depicted in Fig. 5 (χ_M is the magnetic susceptibility for **1** and **2**).

Concerning compound **1**, the effective magnetic moment (μ_{eff}) at room temperature is 4.31 μ_B, very closed to the expected value of 4.00 μ_B for two Ni(II) ions. Upon lowering the temperature, $\chi_M T$ first slowly increases down to about 45 K and then rapidly increases to a value of 2.81 cm^3 K mol^{-1} at 16 K, showing ferromagnetic interactions. Below 16 K, $\chi_M T$ has a rapid drop, which may be attributed to antiferromagnetic exchange interactions or zero-field splitting (ZFS). The whole profile of the $\chi_M T$ *vs.* T curve is indicative of the occurrence of two conflicting effects [36, 37]. Therefore according to the crystal structure, the expression for the magnetic susceptibility ($\chi_M T$) of a Ni(II) dimer derived from Van Vleck's equation (the spin Hamiltonian $\hat{H} = -2J \cdot \hat{S}1 \cdot \hat{S}2$) [38] is expressed in Eq. 1.

$$\chi_M = \frac{2Ng^2\beta^2}{kT}$$

$$\cdot \frac{\left\{ \begin{array}{c} 55+30\exp(-10J/kT)+14\exp(-18J/kT) \\ +5\exp(-24J/kT)+\exp(-28J/kT) \end{array} \right\}}{\left\{ \begin{array}{c} 11+9\exp(-10J/kT)+7\exp(-18J/kT) \\ +5\exp(-24J/kT)+3\exp(-28J/kT) \\ +\exp(-30J/kT) \end{array} \right\}} \quad (1)$$

Considering the molecular field approximation, the total molar magnetic susceptibility takes the form of Eq. 2, where zJ' is the interaction between molecules, and the N, g, β are parameters which have their usual physical meanings.

$$\chi_{\text{tot}} = \frac{\chi_M}{(1-2zj'\chi_M/Ng^2\beta^2)} \quad (2)$$

In order to determine the value of the weak ferromagnetic coupling observed in **2**, we have fitted the high temperature magnetic data ($T > 32$ K). The best-fit parameters obtained are $g = 2.05$, $J = 7.88\,\text{cm}^{-1}$, $zJ' = 1.25\,\text{cm}^{-1}$ with an agreement factor of $R = \Sigma[(\chi_M)^{\text{obs}} - (\chi_M)^{\text{calcd}}]^2/[(\chi_M)^{\text{obs}}]^2 = 8.36 \times 10^{-3}$ for complex **1**.

For compound **2**, the effective magnetic moment at room temperature is 3.29 μ_B, which falls into a reasonable range (2.8 – 3.9 μ_B) for one Ni(II) ion. The value $\chi_M T$ in the range 50 – 300 K displays a slow continuous increase with the decrease of temperature and then a sharp increase when lowering the temperature from 50 to 20 K. Below 20 K, there is a clear decrease of the $\chi_M T$ values. This behavior at low temperature may be a zero-field splitting effect or/and an antiferromagnetic interaction between Ni(II) ions. The magnetic susceptibility data can be analyzed by the following expression based on a Heisenberg Hamiltonian $\hat{H} = -J\sum_{i=1}^{n-1} \hat{S}_i\hat{S}_{i+1}$ ($S = 1$) [39]:

$$\chi_M = \frac{Ng^2\beta^2}{3kT} S(S+1)\frac{1+u}{1-u} + TIP$$
$$u = \coth(JS(S+1)/kT) - kT/(JS(S+1))$$
$$\chi_{\text{tot}} = \frac{\chi_M}{(1-2zj'\chi_M/Ng^2\beta^2)}$$

The best fit from 300 to 25 K leads to $g = 2.01$, $J = 7.32\,\text{cm}^{-1}$, $zJ' = 0.25\,\text{cm}^{-1}$, and an agreement factor $R = \Sigma[(\chi_M)^{\text{obs}} - (\chi_M)^{\text{calcd}}]^2/[(\chi_M)^{\text{obs}}]^2 = 3.59 \times 10^{-3}$ for **2**.

The positive J clearly indicates the existence of a ferromagnetic superexchange for **1** and **2**, possibly *via* 4,4′-bipyridine interactions between adjacent Ni(II) ions, consistent with the magnetic behavior illustrated by the $\chi_M T$ *vs.* T plots.

Conclusion

Two new 4,4′-bipyridine-bridged nickel(II) compounds, dinuclear $[Ni(bpy)_{1.5}(H_2O)_2(BA)_2]\cdot H_2O$ (**1**) and polymeric $[Ni(bpy)(HMBA)(MBA)_2]_n$ (**2**), have been synthesized. The compounds form 3D supramolecular structures formed *via* hydrogen bonds and π-π stacking interactions. The magnetic behavior of **1** and **2** exhibits the occurrence of two complementary couplings between adjacent Ni(II) ions.

Experimental Section

Materials

All chemicals were commercially available in reagent grade and were used without further purification.

Physical methods

Powder X-ray diffraction measurements were carried out with a Bruker D8 Focus X-ray diffractometer to identify the products as well as to check phase purity. The C, H and N microanalyses were performed with a Perkin Elmer 2400II CHN/S elemental analyzer. The FT-IR spectra in the region 4000 – 400 cm^{-1} were recorded at room temperature on pressed KBr discs with a Shimadzu FTIR-8900 spectrometer. Thermogravimetric (TG) measurements, using a Seiko Exstar 6000 TG 6300 apparatus, were conducted from room temperature to 780 °C on preweighed samples in flowing nitrogen with a heating rate of 10 °C min^{-1}. Single-crystal X-ray diffraction data were collected by a Rigaku R-Axis-Rapid X-ray diffractometer. The temperature-dependent magnetic susceptibilities were determined with a Quantum Design SQUID magnetomer (Quantum Design Model MPMS-7) in the temperature range from 2 to 300 K.

*Synthesis of $[Ni(bpy)_{1.5}(H_2O)_2(BA)_2]\cdot H_2O$ (**1**)*

A homogenized mixture of 0.078 g (0.5 mmol) 4,4′-bipyridine (bpy), 0.061 g (0.5 mmol) benzoic acid (HBA), 0.155 g (0.50 mmol) $Ni(NO_3)_2\cdot 6H_2O$, 12 mL H_2O, and 0.1 mL of 7 M NH_4OH was loaded into a 25 mL Teflon-lined stainless-steel autoclave, heated to 180 °C and kept at this temperature for 3 d, and subsequently cooled to room temperature at a rate of 5 K h^{-1}. After filtration and washing with distilled water, 75 mg of green crystals of **1** were separated by hand-picking from the milky-white precipitate (*ca.* 25 % on the basis of the initial $Ni(NO_3)_2\cdot 6H_2O$ input). – Anal. for $C_{29}H_{28}N_3NiO_7$ (%): calcd. C 59.11, H 4.79,

N 7.13; found C 59.31, H 4.92, N 7.25. – XRD (CuK_α, $\lambda = 1.54056$ Å, Fig. S1) data: $(2\theta/I) = 7.50/70$, 13.03/57, 14.32/47, 15.17/100, 17.21/88, 21.43/38, 22.82/30, 24.76/47, 25.15/37, 26.18/36, 26.97/58, 27.78/29. – IR (KBr, cm^{-1}, Fig. S2): ν = 3502(w), 3294(w), 2925(m), 1598(vs), 1556(vs), 1535(s), 1413(s), 1392(vs), 1218(w), 1070(w), 820(m), 721(m).

*Synthesis of [Ni(bpy)(HMBA)(MBA)$_2$]$_n$ (**2**)*

Complex **2** was synthesized analogously to **1** except that 0.061 g (0.5 mmol) *m*-benzoic acid (HMBA) was used instead of 0.069 g (0.5 mmol) benzoic (HBA). After filtration and washing with distilled water, 55 mg (*ca.* 18 % on the basis of the initial $Ni(NO_3)_2 \cdot 6H_2O$ input) green crystals of **2** were separated by hand-picking from the milky-white precipitate and verified to be a pure phase by comparing the experimental PXRD with the simulated one based on the single-crystal data. – Anal. for $C_{34}H_{29}N_2NiO_6$ (%): calcd. C 65.83, H 4.71, N 4.52; found C 65.99, H 7.83, N 4.63. – XRD (CuK_α, $\lambda = 1.54056$ Å, Fig. S1) data: $(2\theta/I) = 7.19/68$, 8.68/12, 11.37/22, 12.50/11, 13.34/9, 15.81/15, 16.57/100, 18.06/14, 18.51/10, 19.62/12, 23.12/25, 24.60/23, 26.70/11, 28.90/15, 30.10/14. – IR (KBr, cm^{-1}, Fig. S2): ν = 3065(w), 2916(w), 1631(s), 1606(vs), 1585(w), 1541(w), 1510(s), 1423(vs), 865(w), 831(w), 761(s), 636(w).

X-Ray structure determinations

Suitable crystals of **1** and **2** were selected under a polarizing microscope and fixed with epoxy cement on fine glass fibers, which were then mounted on a Rigaku R-Axis Rapid IP X-ray diffractometer with graphite-monochromatized MoK_α radiation (λ = 0.71073 Å) for cell determination and subsequent data collection. The data were corrected for Lp and absorption effects. The programs SHELXS-97 and SHELXL-97 were used for structure solution and refinement, respectively [40, 41]. Some non-hydrogen atoms were obtained by using the heavy-atom method, and the subsequent difference Fourier syntheses gave the positions of the remaining non-hydrogen atoms. After several cycles of refinement, some hydrogen atoms associated with carbon atoms were geometrically generated, and the rest of the hydrogen atoms located from successive difference Fourier syntheses. Finally, all non-hydrogen atoms were refined with anisotropic displacement parameters by full-matrix least-squares techniques, and hydrogen atoms refined with isotropic displacement parameters. Detailed information about the crystal data and structure determination is summarized in Table 1. Selected interatomic distances and bond angles are tabulated in Tables 2 and 3.

CCDC 955732 (**1**) and 955733 (**2**) contain the supplementary crystallographic data for this paper. These data can be obtained free of charge from The Cambridge Crystallographic Data Centre *via* www.ccdc.cam.ac.uk/data_request/cif.

Supporting information

Experimental PXRD patterns and diffraction diagrams simulated on the basis of the single-crystal structure determinations for **1** and **2** (Fig. S1), infrared spectra (Fig. S2) and TG curves (Fig. S3) are given as Supporting Information available online (DOI: 10.5560/ZNB.2013-3242).

Acknowledgement

Honest thanks are extended to K. C. Magna Fund in Ningbo University.

[1] J. P. Zhang, X. C. Huang, X. M. Chen, *Chem. Soc. Rev.* **2009**, *38*, 2385 – 2396.
[2] N. N. Adarsh, P. Dastidar, *Chem. Soc. Rev.* **2012**, *41*, 3039 – 3060.
[3] P. Teo, T. S. Hor, *Coord. Chem. Rev.* **2011**, *255*, 273 – 289.
[4] Y. L. Zhu, K. R. Ma, Q. F. Yin, X. D. Zhong, L. Cao, *Polyhedron* **2013**, *63*, 36 – 40.
[5] A. Aslam, I. A. Hashmi, V. U. Ahmed, F. I. Ali, *Synth. Commun.* **2013**, *43*, 2824 – 2831.
[6] B. Przybył, J. Zoń, J. Janczak, *J. Mol. Struct.* **2013**, *1048*, 172 – 178.
[7] H. Y. Sun, C. B. Liu, Y. Cong, M. H. Yu, H. Y. Bai, G. B. Che, *Inorg. Chem. Commun.* **2013**, *35*, 130 – 134.
[8] A. Pop, D. Rosca, R. Mitea, A. Silvestru, *Inorg. Chim. Acta* **2013**, *405*, 235 – 242.
[9] A. Dorazco-González, S. Martinez-Vargas, S. Hernández-Ortega, J. Valdés-Martínez, *CrystEngComm* **2013**, *15*, 5961 – 5968.
[10] H. R. Khavasi, A. A. Tahrani, *CrystEngComm* **2013**, *15*, 5799 – 5812.
[11] Y. B. Shu, C. Xu, W. S. Liu, *Eur. J. Inorg. Chem.* **2013**, *21*, 3592 – 3595.
[12] S. C. Hsu, S. H. Lo, C. C. Kao, C. H. Lin, *Acta Crystallogr.* **2011**, *E67*, m65.
[13] M. A. Nadeem, M. Bhadbhade, R. Bircher, J. A. Stride, *Cryst. Growth Des.* **2010**, *10*, 4060 – 4067.
[14] Y. J. Song, H. Kwak, Y. M. Lee, S. H. Kim, S. H. Lee, B. K. Park, J. Y. Jun, S. M. Yu, C. Kim, S. J. Kim, Y. Kim, *Polyhedron* **2009**, *28*, 1241 – 1252.
[15] K. Biradha, C. Seward, M. J. Zaworotko, *Angew. Chem. Int. Ed.* **1999**, *38*, 493 – 495.

[16] Y. Z. Zheng, Y. B. Zhang, M. L. Tong, W. Xue, X. M. Chen, *Dalton Trans.* **2009**, 1396 – 1406.
[17] E. Y. Choi, Y. U. Kwon, *Inorg. Chem.* **2005**, *44*, 538 – 545.
[18] S. T. Wu, L. S. Long, R. B. Huang, L. S. Zheng, *Cryst. Growth Des.* **2007**, *7*, 1746 – 1752.
[19] X. Y. Li, Y. F. Han, J. K. Li, *Acta Crystallogr.* **2009**, *E65*, m354.
[20] M. Pasquali, C. Floriani, G. Venturi, A. Gaetani-Manfredotti, A. C. Villa, *J. Am. Chem. Soc.* **1982**, *104*, 4092 – 4099.
[21] J. H. Kim, J. M. Bae, H. G. Lee, N. J. Kim, K. Jung, C. Kim, S. Kim, Y. Kim, *Inorg. Chem. Commun.* **2012**, *22*, 1 – 5.
[22] K. S. Gavrilenko, S. V. Punin, O. Cador, S. Golhen, L. Ouahab, V. V. Pavlishchuk, *J. Am. Chem. Soc.* **2005**, *127*, 12246 – 12253.
[23] H. Gong, B. M. Rambo, C. A. Nelson, W. Cho, V. M. Lynch, X. Y. Zhu, Moonhyun Oh, J. L. Sessler, *Dalton Trans.* **2012**, *41*, 1134 – 1137.
[24] O. Kozachuk, K. Khaletskaya, M. Halbherr, A. Betard, M. Meilikhov, R. W. Seidel, B. Jee, A. Poppl, R. A. Fischer, *Eur. J. Inorg.Chem.* **2012**, *10*, 1688 – 1695.
[25] Z. Xu, Y. He, H. Wang. *Z. Naturforsch.* **2012**, *66b*, 899 – 904.
[26] Liu, J. Lang, B. F. Abrahams, *J. Am. Chem. Soc.* **2011**, *133*, 11042 – 11045.
[27] S. Sengupta, S. Ganguly, A. Goswami, S. Bala, S. Bhattacharya, R. Mondal, *CrystEngComm* **2012**, *14*, 7428 – 7437.
[28] J. A. R. Hartmann, S. P. Cooper, *Inorg. Chim. Acta* **1986**, *111*, 43 – 47.
[29] S. C. Hsu, S. H. Lo, C. C. Kao, C. H. Lin, *Acta Crystallogr.* **2011**, *E67*, m65.
[30] X. K. Yu, Y. Q. Zheng, *J. Coord. Chem.* **2013**, *66*, 2208 – 2216.
[31] Y. Q. Zheng, J. L. Lin, *J. Coord. Chem.* **2008**, *61*, 3420 – 3437.
[32] I. Klawitter, S. Meyer, S. Demeshko, F. Meyer, *Z. Naturforsch.* **2013**, *68b*, 458 – 466.
[33] K. Sünkel, D. Reimann, *Z. Naturforsch.* **2013**, *68b*, 546 – 550.
[34] S. Wöhlert, I. Jess, C. Näther, *Z. Naturforsch.* **2012**, *67b*, 41 – 50.
[35] K. Nakamoto, *Infrared and Raman spectra of inorganic and coordination compounds*, 4th ed., John Wiley, New York, **1986**.
[36] F. S. Delgado, M. Hernández-Molina, J. Sanchiz, C. Ruiz-Pérez, Y. Rodríguez-Martín, T. López, F. Lloret, M. Julve, *CrystEngComm* **2004**, *6*, 106 – 111.
[37] X. J. Wang, C. H. Zhan, Y. L. Feng, Y. Z. Lan, J. L. Yin, J. W. Cheng, *CrystEngComm* **2011**, *13*, 684 – 689.
[38] B. W. Sun, S. Gao, B. Q. Ma, D. Z. Niu, Z. M. Wang, *J. Chem. Soc., Dalton Trans.* **2000**, 4187 – 4191.
[39] O. Kahn, *Molecular Magnetism*, VCH Publishers, New York, **1993**.
[40] G. M. Sheldrick, *Acta Crystallogr.* **1990**, *A46*, 467 – 473.
[41] G. M. Sheldrick, *Acta Crystallogr.* **2008**, *A64*, 112 – 122.